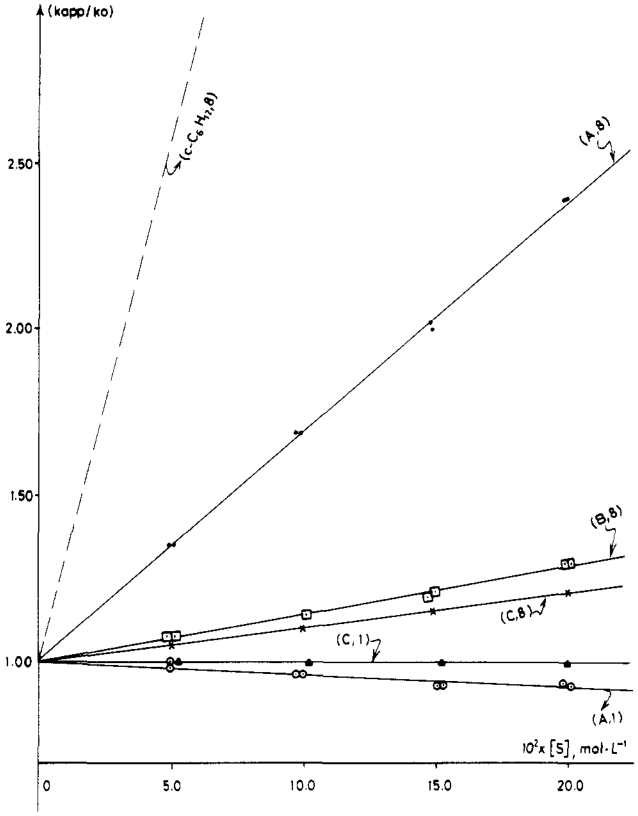

Figure 1. Experimental k_{app}/k_0 values vs cosolvent concentration [S], for reaction 1, in some representative (S_0, S) systems.

selective solvation of the TS by **5** and further illustrates the high catalytic efficiency of aromatic solvents of nil to moderate dipolarity.[1] This is in line with the fact that S_{exp} values are consistently larger in C than in B.

3. The case of mixed solvents (S_0, S) with $\epsilon_S < \epsilon_0$. In these systems, and according to eq 6, S_k is negative, with a minimum at $\epsilon_S = (\epsilon_0 - 1)/2$. For (A, **1**), S_{exp} is indeed negative and the ratio S_{exp}/S_5 equals 1.2. *However, for all the other systems, namely (B, **1**), (B, **2**), (C, **1**), (C, **2**), and (C, **3**), S_{exp} is zero within the limits of experimental error.*[13] *This suggests that, in the latter, the TS is surrounded by and relatively tightly bound to a small*[14] *number of molecules of S_0 and that a reduction of the dielectric constant of the bulk solvent as well as the dilution effect have little bearing on the stability of this solvation shell.* This is reminiscent of findings by Langhals[15] in studies of solvatochromic indicators in mixed solvents. In these studies we are facing the problem of assessing the existence and evaluating the importance of a discontinuous process, the stepwise solvation of a TS, through the comparison of our results with the predictions of the continuous dielectric model. Now, this very model is known to give reasonably good fits of experimental data, even in cases wherein dielectric saturation exists.[16] Hence, clear-cut results are only obtained in the most extreme cases.

Experimental Section

The experimental methodology has been described in detail in part 1 of this series. Relative uncertainties on the k_{app} values are in the 1.0–1.5% range.

Acknowledgment. This work was supported by Grant 0977/84 from CAICYT. Valuable discussions with Prof. M. H. Abraham (University of Surrey, UK) are most appreciated.

Registry No. Et_3N, 121-44-8; MeI, 74-88-4.

---

[13] Most of these systems are near the condition of minimal S_k.

[14] Kondo, Y.; Ohnishi, M.; Tokura, N. *Bull. Chem. Soc. Jpn.* **1972**, *45*, 3579.

[15] Langhals, H. *Angew. Chem., Int. Ed. Engl.* **1982**, *21*, 724.

[16] Ehrenson, S. *J. Am. Chem. Soc.* **1981**, *103*, 6036.

Measured and Computer-Simulated Hydrocarbon and OH Radical Profiles in Fuel-Rich Atmospheric-Pressure Flat Flames. Reactions of CH_4 and C_2H_2

E. W. Kaiser

Chemistry Department, Research Staff, SRL E-3083, Ford Motor Company, Dearborn, Michigan 48121-2053

(Received: July 21, 1989; In Final Form: January 10, 1990)

Density–height profiles of CH_4, C_2H_2, and OH, measured in the postflame gas of rich atmospheric-pressure flat flames fueled by methane, ethylene, acetylene, or propane, are compared to computer-simulated profiles generated by using a 69-reaction kinetic mechanism. In the mechanism chosen for the simulation, the acetylene decays in the postflame gas by reaction primarily with OH with a rate constant determined to be $k_{24} = 9.2\ (\pm 1.5) \times 10^{11}$ cm³/(mol·s) at 1700 K. The superequilibrium pool of partially equilibrated radicals formed in the flame zone decreases toward thermal equilibrium in the postflame gas. Simulation of the OH radical profile shows that recombination of methyl radicals with H atoms controls the shape of this profile and also those of the rest of the free-radical pool. As the acetylene density decreases, the methane density rises. The net methane yield per acetylene consumed varies with the fuel used, reaching 35% for the ethylene flame. This behavior is correctly simulated by using $CH_2CO + H$ as the product of the $C_2H_2 + OH$ reaction, although other mechanistic paths could also be conceived which would yield CH_4. For the acetylene–air flame, densities of allene, methylacetylene, and diacetylene were also measured. These species were near partial equilibrium with the acetylene density at the three heights observed.

Introduction

The high-temperature reactions of methane and acetylene play important roles in combustion, particularly under rich conditions, because of the relatively low reactivity of these molecules. In a previous publication, the chemical kinetics of reactions in the H_2–O_2–CO–CO_2 system were tested by comparing computer-simulated OH profiles to those measured in the postflame gases above laminar atmospheric-pressure flat flames, in which no appreciable concentrations of hydrocarbon species remained.[1] This paper extends those studies to the measured density–height

---

[1] Kaiser, E. W. *J. Phys. Chem.* **1988**, *92*, 4384.

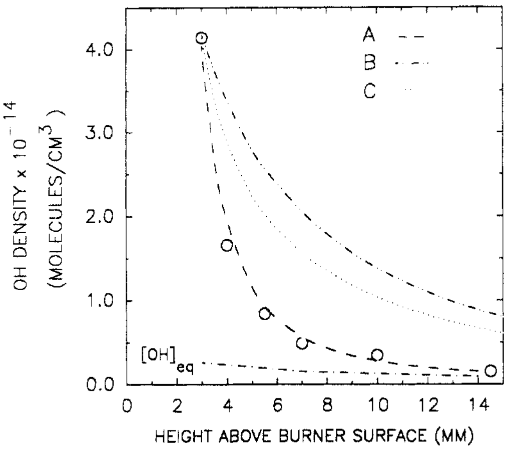

Figure 1. OH profile as a function of height above the burner for a $\phi = 1.46$ propane–air flat flame at 1 atm. Flame zone position = 1.9 mm. Burned gas velocity at 3 mm = 41.5 cm/s. Gas temperature = 1735 K (3-mm height) and 1673 K (10 mm) as shown in ref 2. O_2 density at 3 mm = 3.3×10^{14} molecules/cm^3. Points = experiment; curve A = simulation using rates in Table I; curve B = remove all hydrocarbons from simulation; curve C = remove reactions 7 and 18.

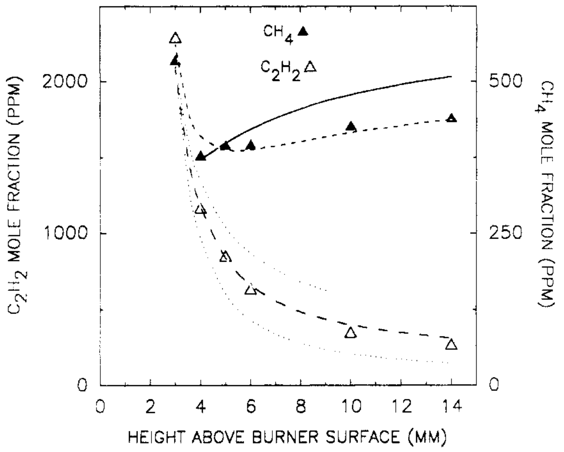

Figure 2. CH_4 and C_2H_2 profiles as functions of height above the burner for the propane–air flame described in Figure 1. Points = experiment; dashed curves = simulation using rates in Table I; dotted curve = multiply k_{24} by 1.5 or 0.67; solid line = multiply k_{15} by 0.67.

profiles of methane, acetylene, selected minor hydrocarbon species, and OH radicals in the postflame gas of rich hydrocarbon–air flames, fueled by propane, methane, acetylene, or ethylene. The temperatures of these flames are cooler than those of similar equivalence ratios in ref 1, and the flames contain ≃200 times larger hydrocarbon concentrations in the postflame region. For a rich propane–air flame at 1700 K, the methane density was observed to increase as the acetylene was consumed in the postflame gas.[2] A possible mechanism for this apparent conversion of acetylene to methane in rich flames will be examined in detail as will the chemical mechanism that determines the rate of decrease toward thermal equilibrium of the superequilibrium radical pool formed in the flame zone.

Experimental Results

Data have been obtained for four (propane, methane, ethylene, and acetylene) hydrocarbon–air flat flames at atmospheric pressure. The operating conditions for each of these flames are summarized in the respective figures. All flames in this study were fuel rich with flame temperatures of 1700–1800 K, and in the following discussions will be identified by the fuel and the fuel–air equivalence ratio (ϕ). This is defined as the ratio of the initial fuel density divided by the air density in the flame of interest to that of the stoichiometric flame for a particular fuel.

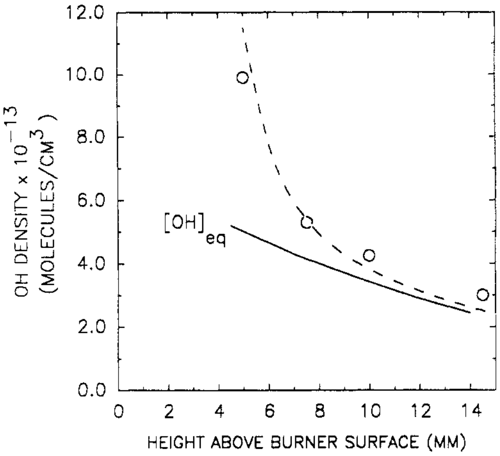

Figure 3. OH profile as a function of height above the burner for a $\phi = 1.5$ methane–air flat flame at 1 atm. Flame zone position = 3.0 mm. Burned gas velocity at 5 mm = 48.6 cm/s. Gas temperature in simulation (see text) = 1793 K (5-mm height) and 1756 K (10 mm). O_2 density at 5 mm = 8×10^{13} molecules/cm^3. Points = experiment; dashed line = simulation using rates in Table I.

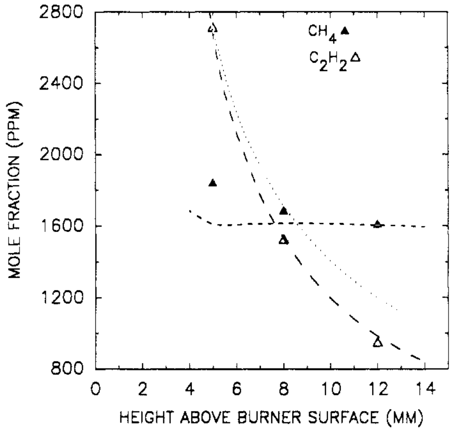

Figure 4. CH_4 and C_2H_2 profiles as functions of height above the burner for the methane–air flame described in Figure 3. Points = experiment; dashed curves = simulation using rates in Table I; dotted curve = multiply k_{24} by 0.72.

Species profiles from a $\phi = 1.46$ propane–air flame are presented in Figures 1 (OH radical) and 2 (CH_4 and C_2H_2). The individual points in these figures represent the experimentally measured species profiles obtained by UV absorption spectroscopy for the OH radical and quartz probe sampling for the stable species. These profiles were presented previously as flame E in ref 2, and the experimental techniques used to obtain these data were discussed in detail in that publication. Three sets of methane and acetylene profiles were presented for this rich flame which differed by ±25% from their mean because of the extreme sensitivity of the profiles of these species to small changes in equivalence ratio.[2] The single set of methane and acetylene profiles chosen from among these three sets for comparison to the simulated curves was that designated by circles in ref 2 and was obtained by using conditions most closely matching those under which the OH profile was determined. The methane and acetylene densities in ref 2 were presented under partially dried conditions. Those data have been corrected to obtain the profiles in Figure 2 for which no water condensation has occurred. A complete temperature profile in the postflame gas was determined by a radiation-corrected thermocouple measurement.[2] The temperatures used in the simulation at two heights above the burner are included in the relevant figure caption for reference. Volume flow rates were measured by a rotameter[2] to calculate the flow velocity for the simulation. Note that this flame has a slower cold gas flow velocity and, therefore, a lower temperature than that of the flame with a similar equivalence ratio that was simulated in ref

---

[2] Kaiser, E. W.; Marko, K.; Klick, D.; Rimai, L.; Wang, C. C.; Shirinzadeh, B.; Zhou, D. *Combust. Sci. Technol.* **1986**, *50*, 163.

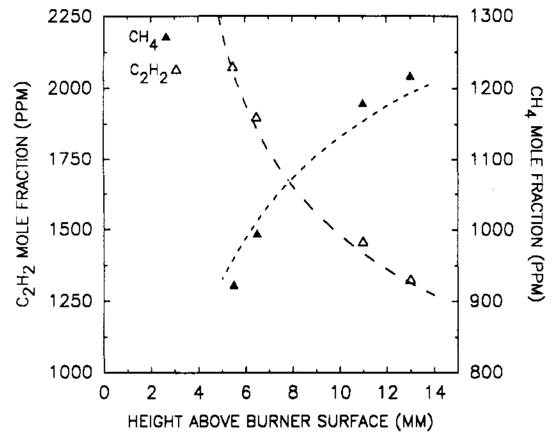

Figure 5. CH_4 and C_2H_2 profiles as functions of height above the burner for a $\phi = 1.5$ ethylene–air flat flame at 1 atm. Flame zone position = 1.5 mm. Burned gas velocity at 5 mm = 45.9 cm/s. Gas temperature in simulation (see text) = 1714 K (5-mm height) and 1684 K (10 mm). O_2 density at 5 mm = 2.5×10^{13} molecules/cm^3. Points = experiment; dashed lines = simulation using rates in Table I.

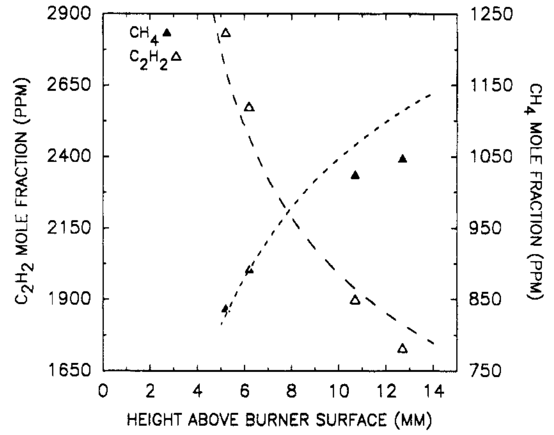

Figure 6. CH_4 and C_2H_2 profiles as functions of height above the burner for a $\phi = 1.5$ acetylene–air flat flame at 1 atm. Flame zone position = 1.2 mm. Burned gas velocity at 5 mm = 45.5 cm/s. Gas temperature in simulation (see text) = 1719 K (5-mm height) and 1689 K (10 mm). O_2 density at 5 mm = 2.2×10^{13} molecules/cm^3. Points = experiment; dashed lines = simulation using rates in Table I.

1. This lower temperature results in hydrocarbon densities in the postflame gases, which are 200 times greater.

In Figures 3 and 4, the individual points represent the measured OH, C_2H_2, and CH_4 profiles for a fuel-rich ($\phi = 1.5$) methane–air flame at atmospheric pressure obtained by the same techniques as described for the propane flame. Figures 5 and 6 present the methane and acetylene profiles for $\phi = 1.5$ ethylene– and acetylene–air flames at atmospheric pressure. No OH profiles were obtained for these latter two fuels.

Two major features of the experimentally measured profiles are of particular importance. First, for both the methane and propane flames, the OH radical is formed in the flame zone at a density above thermal equilibrium as shown in Figures 1 and 3. In the propane–air flame, a density 16 times larger than equilibrium is observed at a height 3 mm above the burner surface (1.6 mm above the luminous flame zone). As has been demonstrated,[1] simulation of the decay of OH toward equilibrium can provide important information about critical free-radical recombination reactions at high temperature, which determine the shape of the OH radical decay profile. Second, for all flames, the acetylene density decreases substantially in the postflame gas. As the acetylene is consumed, methane is formed with a net yield which varies with the fuel used but reaches a maximum of 35% for the ethylene flame. An increase in methane density was noted previously[2] but is much larger in absolute magnitude for the ethylene and acetylene flames. This supports the conclusion that acetylene is converted to methane by reactions occurring within the postflame gas, an important observation that will be examined in detail by computer simulation.

Simulation Procedure

Use of the HCT (Hydrodynamics, Chemistry and Transport) code, developed at Lawrence Livermore National Laboratory, to generate simulated computer species profiles in the postflame gas of flat flames has been described in detail.[1] Briefly, the initial concentrations of stable hydrocarbons and of OH were fixed in the simulation at their measured values at an initial point in the postflame gas. The simulated changes in the species mole fractions with increasing height above the burner were then compared to the measured profiles to test the chemical kinetic mechanism used in the simulation.

The experimentally measured densities of CO and CO_2 remained nearly constant at their equilibrium values in this region of the postflame gas and were used in the calculation. The densities of H_2O and H_2 were not measured. The initial values were, therefore, adjusted in the simulation such that their calculated equilibrium mole fractions were reached at a position approximately 1 cm above the burner surface. Over the height range simulated, the computed H_2 and H_2O densities changed less than 4%. The mole fraction of O_2 in the postflame gas was too small to be measured for all but the propane flame. In the propane–air flame the measured O_2 mole fraction at a height 2.5 mm above the burner was 0.005, while at 3 mm, it had fallen to below the detection limit of $\simeq 0.0005$. Thus, in the postflame gases of these flames, the O_2 density is small and rapidly decreasing. The effect of variation of initial O_2 density on the simulated profiles was tested only in the case of the propane–air flame. In this flame, an initial O_2 density 7 times larger at 3-mm height than that used to generate Figures 1 and 2 was also used in a simulation. The increased initial O_2 produced small changes in the first 2 mm of the simulation, increasing the OH by 8% and the CH_4 by 40% at 3-mm height. However, for distances greater than 5 mm, the profiles were nearly identical. Thus, changes of this magnitude in the initial O_2 produce only a small effect in the initial portions of the simulated propane–air profiles. For the C_2H_4, C_2H_2, and CH_4 flames, the initial O_2 density at the first point for which data are available should be even smaller than in the propane flame. In these flames, the initial heights for which species densities were measured are farther from the flame front, and the predicted O_2 density is decreasing approximately a factor of 3–10 per millimeter increase in height. The initial O_2 density assumed for each of the flames is presented in the caption of the appropriate figures.

The radiation-corrected temperature profile measured in the burned gas by a Pt/Pt(13% Rh) thermocouple was used directly in the simulation for the propane–air flame. Temperature profiles for the acetylene, ethylene, and methane–air flames were adjusted within their measurement error limits (±30 K) to achieve a better fit to selected species profiles as will be discussed. Initial flow velocities in the postflame gas were calculated from the measured cold gas flow and temperature. The diffusion coefficients presented previously[1] were used in the simulation, except for that of the H atom, whose diffusion coefficient was increased by 14% at all temperatures to achieve better agreement with measurements[3,4] at room temperature.

The reaction set used in the simulation is presented in Table I and with the exception of reaction 24, which is fitted in this simulation, and reactions 15 and 53, which were adjusted by $\simeq$50% from literature values, represents an evaluation of the best rates for the reactions available in the literature and, in certain cases to be discussed, a choice of possible product channels.

OH Profiles. If one uses the rates in Table I, the simulated profile of OH as it decreases toward thermal equilibrium in the propane–air flame (curve A in Figure 1) deviates by less than 20% from the experimental data, which span a density range of a factor of 20. This agreement is within the experimental error limits.

---

(3) Lynch, K. P.; Michael, J. V. *Int. J. Chem. Kinet.* **1978**, *10*, 233.
(4) Mason, R. S.; Clifford, A. A.; Gray, P.; Waddicor, J. I. *Proc. Symp. Thermophys. Prop.* **1982**, *8th* (1), 281.

TABLE I: Reaction Mechanism for Simulation of Postflame Species Profiles

	forward[a]			reverse[a]			
reaction	log *A*	*b*	*E*	log *A*	*b*	*E*	ref[b]
1. $H + O_2 = O + OH$	14.39	0	17272	13.28	0	1 157	1
2. $O + H_2 = H + OH$	4.03	2.8	5921	3.68	2.8	3 826	1
3. $OH + OH = H_2O + O$	8.32	1.4	−397	9.32	1.4	16 850	1
4. $OH + H_2 = H_2O + H$	13.68	0	6092	14.31	0	21 250	1
5. $H + OH + M = H_2O + M$	22.34	−2.0	0	27.25	−3.0	122 600	1
6. $H + H + M = H_2 + M$	18.73	−1.3	0	23.01	−2.3	107 400	1
7. $CH_4 + M = CH_3 + H + M$[c]	17.67	0	93170	11.95	1.0	−15 040	5
8. $CH_4 + H = CH_3 + H_2$	4.35	3.0	8755	2.94	3.0	8 275	6
9. $CH_4 + OH = CH_3 + H_2O$	5.29	2.4	2120	4.50	2.4	16 800	6
10. $CH_3 + O_2 = CH_3O + O$	13.38	0	29000	14.18	0	733	16
11. $CH_3 + O = CH_2O + H$	13.85	0	0	14.97	0	69 630	14
12. $CH_3 + HCO = CH_4 + CO$	14.08	0	0	16.31	0	89 050	6
13. $CH_3 + OH = CH_2 + H_2O$	13.18	0	5000	13.12	0	15 450	17
14. $CH_3 + H = CH_2 + H_2$	13.95	0	15200	13.26	0	10 500	17
15. $CH_3 + OH \rightarrow CH_2OH + H$	13.94	0	6190	0.0	0	0	text, 6, 15
16. $CH_3 + CH_3 = C_2H_6$	53.23	−12.0	19500	60.15	−13.0	110 100	32 (1 atm)
17. $CH_3 + CH_2O = CH_4 + HCO$	3.74	2.81	5862	4.06	2.81	22 440	6
18. $CH_3OH + M = CH_3 + OH + M$	17.28	0	73570	11.26	1.0	−19 770	18
19. $CH_2 + H = CH + H_2$	13.60	0	0	13.45	0	2 990	14
20. $CH_2 + OH = CH_2O + H$	13.48	0	0	15.65	0	76 430	est, 6
21. $CH + H = C + H_2$	14.18	0	0	14.78	0	23 820	17
22. $CH + CO_2 = HCO + CO$	12.53	0	690	11.71	0	67 890	19
23. $C + CO_2 = CO + CO$	12.48	0	5100	11.86	0	137 000	20, *d*
24. $C_2H_2 + OH = CH_2CO + H$	13.51	0	12000	14.50	0	32 660	text, 7–11
25. $C_2H_2 + O = HCCO + H$	14.60	0	10660	15.11	0	32 090	21
26. $C_2H_2 + O = CH_2 + CO$	14.20	0	9885	13.48	0	60 560	21
27. $C_2H + H_2 = C_2H_2 + H$	13.06	0	2880	13.96	0	23 350	6
28. $C_2H_2 + OH = C_2H + H_2O$	12.78	0	7000	12.51	0	1 685	16
29. $C_2H_2 + M = C_2H + H + M$	16.90	0	106900	11.72	1.0	−20 970	est, 6, 14
30. $C_2H_2 + C_2H = C_4H_2 + H$	13.54	0	0	14.82	0	15 190	14
31. $pC_3H_4 + H = CH_3 + C_2H_2$	13.30	0	0	12.52	0	11 050	22
32. $C_2H_3 + M = C_2H_2 + H + M$	41.62	−7.49	45540	37.71	−6.49	4 706	6 (1 atm)
33. $C_2H_4 + H = C_2H_3 + H_2$	7.18	2.0	6000	6.02	2.0	2 954	16
34. $C_2H_4 + OH = C_2H_3 + H_2O$	13.30	0	5960	12.78	0	18 070	23
35. $C_2H_4 + M = C_2H_3 + H + M$	18.80	0	108700	13.37	1.0	−1 786	16
36. $C_2H_4 + OH = CH_3 + CH_2O$	11.26	0	0	11.08	0	16 360	est
37. $C_2H_5 = C_2H_4 + H$	43.41	−9.25	52660	40.09	−8.25	14 220	32 (1 atm)
38. $C_2H_6 + OH = C_2H_5 + H_2O$	9.93	1.05	1810	8.75	1.05	20 790	24
39. $C_2H_5 + H = C_2H_6$	11.58	0	0	17.68	−1.0	103 600	6 (1 atm, 1700 K)
40. $C_2H_6 + H = C_2H_5 + H_2$	2.73	3.5	5200	0.91	3.5	9 030	16
41. $CH_3 + CH_3 = C_2H_5 + H$	12.70	0.1	10600	13.52	0.1	−2 420	25
42. $pC_3H_4 + H = C_3H_3 + H_2$	2.43	3.5	5200	2.24	3.5	20 860	est, see (40)
43. $pC_3H_4 + OH = C_3H_3 + H_2O$	9.64	1.05	1810	10.10	1.05	32 620	est, see (38)
44. $aC_3H_4 + H = C_3H_3 + H_2$	7.18	2.0	6000	6.73	2.0	23 050	est, see (33)
45. $aC_3H_4 + OH = C_3H_3 + H_2O$	13.30	0	5960	13.49	0	38 160	est, see (34)
46. $aC_3H_4 + OH = CH_2CO + CH_3$	12.24	0	−300	12.19	0	32 800	26, *e*
47. $aC_3H_4 + OH = C_2H_3 + CH_2O$	12.24	0	−300	12.31	0	17 250	26, *e*
48. $pC_3H_4 + OH = CH_2CO + CH_3$	12.57	0	0	12.78	0	31 710	26, *f*
49. $aC_3H_4 = pC_3H_4$	8.40	0	36220	8.14	0	37 610	27, *g*
50. $C_4H_2 + OH = C_3H_3 + CO$	12.52	0	−410	13.07	0	66 940	28, *h*
51. $C_4H_2 + OH = C_2H_2 + HCCO$	12.52	0	−410	13.01	0	28 400	28, *h*
52. $CH_2CO + H = CH_3 + CO$	13.55	0	4007	12.88	0	40 810	text, 14, 31
53. $CH_2CO + OH = CH_2O + HCO$	14.12	0	1526	14.11	0	21 480	text, 29, 30
54. $CH_2CO + M = CH_2 + CO + M$	15.56	0	59300	9.92	1.0	−16 040	14
55. $HCCO + OH = HCO + HCO$	13.00	0	0	12.02	0	33 190	17
56. $HCCO + H = CH_2 + CO$	14.00	0	0	12.76	0	29 240	17
57. $CH_2OH + H = CH_2O + H_2$	13.48	0	0	19.89	−1.66	80 000	14
58. $CH_2OH + OH = CH_2O + H_2O$	13.48	0	0	20.52	−1.66	95 180	est, see (57)
59. $CH_2OH + M = CH_2O + H + M$[c]	37.60	−6.65	33270	39.73	−7.31	5 854	est, see (67)
60. $CH_2OH + H_2 = CH_3OH + H$	7.50	1.66	15160	13.48	0	7 000	16
61. $OH + CO = H + CO_2$	7.18	1.3	−765	9.26	1.3	21 420	1
62. $H + CO + M = HCO + M$	20.80	−1.82	3688	24.31	−2.82	22 916	1
63. $OH + HCO = H_2O + CO$	14.00	0	0	15.41	0	103 346	1
64. $H + HCO = H_2 + CO$	13.84	0	0	14.57	0	88 164	1
65. $CH_2O + OH = HCO + H_2O$	12.86	0	170	12.41	0	29 990	16
66. $CH_2O + H = HCO + H_2$	13.40	0	4000	12.30	0	20 100	14
67. $CH_3O + M = CH_2O + H + M$	37.60	−6.65	33270	39.73	−7.31	5 854	6
68. $CH_3O + H = CH_2O + H_2$	13.30	0	0	12.87	0	83 880	14
69. $CH_3O + OH = CH_2O + H_2O$	13.00	0	0	13.20	0	99 000	est, see (69)

[a] Units: mol/cm^3, s, kcal; $k = AT^b \exp(-E/RT)$. [b] References are for the forward rate constants; most reverse rate constants are calculated from thermodynamic data contained in the JANAF tables supplemented by data from refs 6, 33, and 34 and are valid for $T \geq 1000$ K. Numbers in parentheses refer to reactions in the table. [c] Relative third-body efficiencies estimated to be the following: H_2, 2; H_2O, 7.5; CO_2, 2; all others, 1. Rate constant valid for $T \geq 1600$ K and 1 atm. [d] Estimated from upper limit at 300 K. [e] Low-temperature rate split between two possible product channels. [f] 298 K; assumed product channel. [g] 1500–1800 K at 1 atm; aC_3H_4 = allene, pC_3H_4 = propyne. [h] Split between two possible product channels.

The simulation predicts that the OH, H, and O densities as well as the densities of certain hydrocarbon radicals (e.g., C_2H, CH_3, CH_2) are within 10% of partial equilibrium with one another and with the stable hydrocarbon species throughout the postflame region. As stated previously,[2] the observed rate of decrease of the OH radical density toward thermal equilibrium in the postflame gas is much faster than can be explained by the sum of the direct recombination reactions 5 and 6, which determines the OH profile for the higher temperature propane–air flame of the same equivalence ratio in which hydrocarbon molecules are absent.[1]

To determine which reactions contribute significantly to the decay of the partially equilibrated free-radical pool, selected individual reactions were removed from the simulation to establish the extent of their influence on the OH profile in the propane–air flame. By use of this sensitivity analysis, the recombination of H atoms with methyl radicals (reaction −7) was determined to be the most important single reaction affecting the OH profile. Reaction −7 combined with reaction 8, which is near partial equilibrium, effectively produces a methyl-radical-catalyzed recombination of H atoms. As shown in Figure 1 (curve C), removal of both this reaction and the similar recombination of OH with CH_3 (reaction −18) decreases the observed initial slope of the OH radical profile by 50% (with reaction −7 producing approximately 90% of this decrease). The chemical contribution of these two reactions to the decay of the radical pool is actually $\simeq 75\%$ because of the effect of diffusion on the species profiles. H atoms are partially equilibrated with the OH radicals and are present in 8-fold greater concentration. For this reason, the effective diffusion velocity of OH is controlled largely by the diffusion of H atoms, and diffusion provides approximately 85% of the apparent velocity of the OH radicals in the flame at a height 3.5 mm above the burner. Removing reactions 7 and 18 from the mechanism decreases the slope of the simulated profile which in turn reduces the calculated diffusion velocity. This reduced velocity increases the slope of curve C relative to that of curve A, making the apparent change in the slope smaller than the true change in the OH chemical consumption rate when these reactions are removed.

The rate constant, k_{-7}, used in the simulation is derived by thermodynamics from the value of k_7 measured by Roth and Just.[5] Their value was determined under conditions of temperature and pressure nearly approximating those of our measurements. However, all measurements of this rate constant in the 0.5–2.0-atm range at 1700–1800 K are in reasonable agreement.[6] No measurement of the third-body efficiencies for this reaction are available to our knowledge. The efficiencies used represent estimates. Note that the temperature dependence of reaction 7 in Table I is valid only in the high-temperature atmospheric-pressure regime in which it was determined by Roth and Just.

Setting all hydrocarbon concentrations to zero in the simulation to assess the effect of all hydrocarbon reactions together on the OH profile produces curve B in Figure 1. The additional reduction in the OH decay rate indicates that hydrocarbon reactions other than (7) and (18) contribute approximately 20% to the chemical rate of OH removal. The residual decay of OH in the simulation curve B shows that direct recombination reactions

$$H + OH + M = H_2O + M \tag{5}$$

$$H + H + M = H_2 + M \tag{6}$$

produce only $\simeq 5\%$ of the initial chemical decay rate of the OH radical as verified by removal of reactions 5 and 6.

The measured OH profile for the methane–air flame in Figure 3 is not suitable for testing the radical recombination mechanism accurately because the measured OH density is never more than a factor of 2 larger than the equilibrium density over the height range measured. This makes the calculated OH profile very sensitive to the accuracy of the temperature determination in contrast to the propane–air flame. For this reason, in order to obtain a simulated OH decay curve that agrees to within experimental error with that measured, the temperature profile used in the simulation was increased by 15 K above that determined experimentally; this adjustment is less than the error (±30 K) estimated for the temperature measurement. The temperature change increased the simulated OH density approximately 20% at a height 10 mm above the burner surface. Obtaining a satisfactory simulated OH profile using this method allows a better test of other kinetic parameters in the mechanism using the methane–air data.

C_2H_2 Profiles. The excellent agreement between the simulated and measured OH profiles in the propane– and methane–air flames permits the testing of portions of the mechanism that involve reactions between OH and the major hydrocarbon species. Previously, an analysis of the OH and C_2H_2 profiles in the propane–air flame showed that the rate of acetylene consumption in the postflame region was directly proportional to the OH density.[2] This indicates either that C_2H_2 is consumed by direct reaction with OH to form irreversible products (e.g., reaction 24) or that intermediate radical products such as C_2H or C_2H_3, formed in reactions with H or OH [e.g., (28) and (−32)], are consumed rapidly to yield final products. Since H and OH are in partial equilibrium in these flames, the C_2H_2 decay rate would be proportional to OH in both cases.

Net consumption of such a radical intermediate via reaction with another radical species would result in a greater than first-order dependence of the C_2H_2 decay rate on the OH density and would not fit the experimental data, in which this decay rate is proportional to the first power of the OH concentration. It is possible, however, that in the case of C_2H_2 consumption via an intermediate radical, the C_2H or C_2H_3 reacts rapidly with one of the major product species (such as H_2O), which have constant densities in the postflame gas. Two examples of exothermic overall reactions of this type, leading to a decay curve which is directly proportional to the OH concentration, could be

$$C_2H + H_2O \rightarrow CH_3 + CO \tag{A}$$

$$C_2H_3 + H_2O \rightarrow CH_3 + CO + H_2 \tag{B}$$

Both of these reactions would consume C_2H_2 and form CH_3 as required by the experimental data.

The current flame measurements cannot distinguish between the two types of C_2H_2 consumption mechanisms (direct or via radical intermediate), but for the purpose of the simulation, we have assumed that C_2H_2 is consumed in a direct reaction with OH. The rate constant for the assumed reaction, (24), was derived

$$C_2H_2 + OH \rightarrow CH_2CO + H \tag{24}$$

in the simulation by adjusting its value until a satisfactory fit to the measured C_2H_2 profile was obtained for the propane–air flame (see Figure 2). Changing the rate constant of reaction 24 by ±50% produced a significant deviation from the observed C_2H_2 profile as shown by the dotted lines in the figure, indicating that the accuracy of this determination of k_{24} is approximately ±15%. The good agreement with the observed C_2H_2 profile for the methane–air flame data shown in Figure 4 also supports this value of the rate constant.

The value of k_{24} deduced at 1700 K, which is the average temperature of the postflame gas region for the propane–air flame, is $9.2\ (\pm 1.5) \times 10^{11}$ cm^3/(mol·s) and at 1770 K, the average temperature in the methane–air flame, is $1.1\ (\pm 0.15) \times 10^{12}$ cm^3/(mol·s). As shown in Figure 7, these values agree satisfactorily with two other high-temperature measurements deduced from atmospheric-pressure flames[7,8] and with an extrapolation of the rate constants measured over the temperature range 1050–1400 K by Smith et al.[9] in a reduced pressure (50–300 Torr) study of the kinetics of the individual reaction, $OH + C_2H_2 \rightarrow$

---

[5] Roth, P.; Just, Th. *Ber. Bunsen-Ges. Phys. Chem.* **1975**, *79*, 682.

[6] Tsang, W.; Hampson, R. F. *J. Phys. Chem. Ref. Data* **1986**, *15*, 1087.

[7] Fenimore, C. P.; Jones, G. W. *J. Chem. Phys.* **1964**, *41*, 1887.

[8] Bittner, J. D.; Howard, J. B. *Symp. (Int.) Combust.*, *[Proc.]*, *19th* **1983**, 211.

[9] Smith, G. P.; Fairchild, P. W.; Crosley, D. R. *J. Chem. Phys.* **1984**, *81*, 2667.

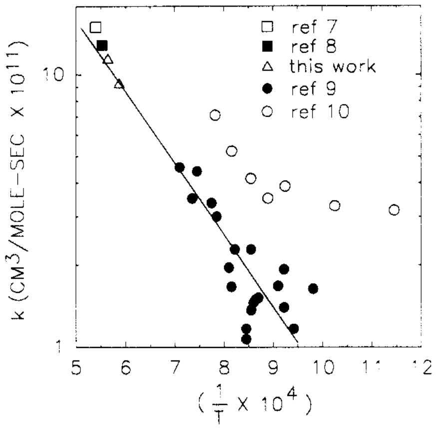

Figure 7. Measured values of the rate constant for the reaction OH + C_2H_2 → products for $T \geq 1000$ K. Solid line represents rate constant of reaction 24 in Table I.

products. The high-temperature atmospheric-pressure rate constants of Liu et al.[10] are approximately a factor of 2 larger than the data of Smith et al. for unknown reasons, possibly involving a contribution from the pressure-dependent addition reaction in their higher pressure experiments, but show a similar temperature dependence. The low-pressure flame data of Browne et al.[11] also agree with the other flame measurements although there may be some difficulty with their data interpretation.[8] The rate constant attributed to Fenimore and Jones[7] in Figure 7 has been recalculated based on data in their Figure 2 and more recent thermodynamic parameters in the JANAF tables. The new value (1.5×10^{12} cm^3/(mol·s)) at their average temperature of 1860 K lies approximately 25% lower than their stated value. There is good agreement between the several indirect high-temperature flame determinations of this rate constant and the extrapolation of the temperature dependence measured directly for the individual reaction between 1050 and 1400 K by Smith et al.[9] This agreement lends support to the supposition that all of these measurements have determined the rate constant of the same reaction between OH and C_2H_2 over this temperature range despite questions regarding the products formed.

Smith et al.[9] believe the product to be C_2H based on the fact that there is a positive activation energy as might be expected of an abstraction reaction. Calculations by Miller and Melius[12] support this product choice. Bittner and Howard,[8] however, suggest the formation of ketene because they observe a mass peak at 42 amu in their mass spectrometer, agreeing with the ketene mechanism presented by Levy and Sarofim.[13a] The next section explores a possible product channel that can explain the measured methane profiles, shedding additional light on the mechanism.

OH profiles were not measured for the C_2H_4 or C_2H_2 flames. However, the above data for the propane and methane flames have shown that C_2H_2 decays at a rate directly proportional to the OH density in these rich flames, and therefore, the C_2H_2 profile can be used to estimate the profiles of the free-radical pool which is partially equilibrated with OH. In order to simulate data from these two flames, the OH profile for each flame was varied until the simulated acetylene decay rate agreed with the experimental data. In this procedure, the initial OH density at 5 mm above the burner and the temperature profile were adjusted to attain the required experimental C_2H_2 profile. For both flames, the temperature was increased by 30 K above that measured, which is equal to the estimated uncertainty in the temperature measurement. This technique then permits the testing of the CH_4 generation mechanism using the data from these flames even in the absence of OH measurements.

CH_4 Profiles. As the acetylene is consumed in the postflame gas of the propane–air flame, the methane density rises (see Figure 2). For this flame, the rise is small in absolute magnitude ($\simeq$70 ppm) but significant in terms of the experimental error as shown by repeat measurements at slightly different equivalence ratios.[2] The increases in methane mole fraction observed in the acetylene–air (Figure 5) and ethylene–air (Figure 6) flames are considerably larger, reaching 300 ppm for the ethylene–air flame, far greater than the experimental measurement error. Thus, as mentioned previously, there must be a mechanism by which acetylene is converted to methane in the postflame gas of these rich flames.

The formation of ketene by an exothermic reaction between OH and acetylene has been suggested by Levy and Sarofim[13a] as a way to improve calculated fits to experimental flame data. Ketene has been observed as the sole product in a low-pressure, room-temperature, molecular-beam study of the C_2H_2 + OH reaction,[13b] and Bittner and Howard[8] observed a mass peak at 42 amu, which could arise from ketene, in their study of benzene flames. There are no other data regarding products from this reaction of which we are aware. Based on these limited results, the products chosen for reaction 24 in this simulation are ketene and an H atom. Ketene subsequently will react with H atoms and OH radicals in the postflame gas to give final reaction products. Again, direct determinations of the products formed by these reactions are not available; we have chosen the paths shown in Table I for reactions 52 and 53, which have been suggested previously.[14] Reaction of ketene with H atoms (52) yields methyl radicals and, therefore, provides a source of methane formation from the C_2H_2 + OH reaction as is required to fit the data in Figures 2 and 4–6. The rate constant for reaction 52 was derived from an Arrhenius plot of all of the available data referenced in Table I. Rate data for reaction 53 are much sparser. The rate constant k_{53} was derived from the two available data sets but with a 50% increase at 1700 K to provide the best fit possible to the methane yield data in Figures 1–6 as discussed in the next paragraph. This modest increase still fits all data to within the scatter of the experiments.

We emphasize that the choice of ketene as the product for reaction 24 is not the only possible choice, and in fact, theoretical calculations by Miller and Melius[12] do not support this as the major product channel. It is possible that reaction 24 forms C_2H, which subsequently reacts with a stable product such as H_2O to yield a methane precursor. Such a reaction mechanism could also explain our experimental data, but to our knowledge no such reaction of C_2H radicals has been identified. Additional experiments are required to clarify this portion of the mechanism.

Another important reaction controlling the shape of the simulated methane profile is

$$CH_3 + OH \rightarrow CH_2OH + H \qquad (15)$$

which is the primary reaction removing methane in the simulation. Neither the rate constant nor the products of this reaction are well established at high temperature. In the simulation, CH_2OH + H are the assumed products as suggested by Tsang and Hampson.[6] The value of k_{15} at 1700 K (1.4×10^{13} cm^3/(mol·s)) was determined by varying the rate constant to give the best overall fit to the CH_4 profiles in all four flames. The sensitivity of the computed CH_4 profile in the propane–air flame to the value of this rate constant is illustrated by the solid curve in Figure 2, which was obtained by decreasing k_{15} by 30%. A rate constant ($k_{15} = 9 \times 10^{14} \exp(-15500/RT)$), which agrees to within 50% with the above value at 1700 K, has been estimated from shock-heated reacting mixtures of methane and oxygen over the temperature range 1850–2500 K, with the bulk of the measurements made at 1900–2200 K.[15] The temperature dependence of the rate constant

---

[10] Liu, A.; Mulac, W. A.; Jonah, C. D. *J. Phys. Chem.* **1988**, *92*, 5942.

[11] Browne, W. G.; Porter, R. P.; Verlin, J. D.; Clark, A. H. *Symp. (Int.) Combust., [Proc.], 12th* **1969**, 1035.

[12] Miller, J. A.; Melius, C. F. *Symp. (Int.) Combust., [Proc.], 22nd* **1989**, 1031.

[13] (a) Levy, J. M.; Sarofim, A. F. *Combust. Flame* **1983**, *53*, 1. (b) Kanofsky, J. R.; Lucas, D.; Pruss, F.; Gutman, D. *J. Phys. Chem.* **1974**, *78*, 311.

[14] Warnatz, J. In *Combustion Chemistry*; Gardiner, W. C., Ed.; Springer-Verlag: New York, 1984; p 197.

[15] Roth, P.; Just, Th. *Symp. (Int.) Combust., [Proc.], 20th* **1985**, 807.

TABLE II: Mole Fraction (ppm) of Minor Hydrocarbon Species in the Acetylene–Air Flame[a]

height above burner, mm	C_2H_6	C_2H_4	aC_3H_4	pC_3H_4	C_4H_2
5.2	10 ± 1	14 ± 1	2.9 ± 0.6	7 ± 1.4	24 ± 4
	0.7	8.5	3.5	9.5	17.6
6.2	8	12	2.4	7	21
	0.5	7.2	3.3	9.0	14.3
10.8	7	9	1.8	4.7	9
	0.3	5.6	3.0	7.8	9.0
12.8	7	9	1.7	4.2	
	0.3	5.5	2.7	7.5	7.0

[a] Upper entries are experimental data. Lower entries are simulated.

presented in Table I was obtained from the value of k_{15} at 1700 K derived from the present simulations and that determined at the average temperature (2000 K) of the Roth and Just experiments.[15] This yields a rate constant with a lower activation energy than estimated by Roth and Just. As observed by Tsang and Hampson, it is difficult to explain a very high activation energy for this radical–radical reaction. The CH_4 profiles are also influenced by the net methane yield as determined by the relative rates of reactions 52 and 53. The rates of reactions 15, 52, and 53 presented in Table I, therefore, represent a set which provides a satisfactory fit to the flame data in Figures 2 and 4–6, but the individual rate constants may not be determined uniquely.

Minor Hydrocarbon Species. In addition to the major species, CH_4 and C_2H_2, several other hydrocarbons (ethane, ethene, allene (aC_3H_4), propyne (pC_3H_4), and diacetylene) were observed at much lower densitites. The concentrations of these species are compared in Table II to the simulated values for the acetylene flame, in which the concentrations were sufficiently large to be measured with 20% or better accuracy. For allene, propyne, and diacetylene, the simulation predicts that the species are equilibrated with acetylene in the postflame gas. The agreement with the observed densities is reasonable, probably within current knowledge of the thermodynamic properties for these species, verifying that they are partially equilibrated with acetylene.

However, the observed density of ethane is typically 15 times larger, while that of ethylene is 1.6 times larger than predicted. It is probable that the excess ethane and ethylene result from methyl radical recombination or disproportionation reactions occurring within the probe during sampling. At a height 5.2 mm above the burner surface, the predicted methyl radical mole fraction is 60 ppm in the acetylene flame. Thus, the excess ethylene (5 ppm) and the ethane (9 ppm) can account for approximately half of the methyl radical present in the hot flame gases. The remainder could undergo reaction with either H_2 or H atoms to form 30 ppm of methane during the sampling process, an amount which is small in comparison to the methane density in the burned gas. Thus, only measurements of the ethane and possibly the ethylene densities are likely to be perturbed signficantly by radical recombination reactions in the probe.

Conclusions

A combined computational and experimental study of hydrocarbon and OH radical profiles as functions of height above the burner surface has been carried out in the postflame burned gas region of four (CH_4, C_2H_2, C_2H_4, C_3H_8) fuel-rich flat flames at atmospheric pressure. The mechanism in Table I predicts the observed density profiles of the major hydrocarbons, CH_4 and C_2H_2, and of OH to better than 15% for all flames. Minor hydrocarbons (allene, propyne, and diacetylene) are partially equilibrated with C_2H_2 to within experimental error for the acetylene flame, in which they could be observed accurately.

The decay of the OH radical is correctly simulated in the propane–air flame over a factor of 20 decrease in density. A sensitivity analysis reveals that the recombination of H atoms with methyl radicals is the most important reaction controlling the profile shape because the OH radicals are partially equilibrated with H atoms. Based on a review of references currently available in the literature, acetylene is consumed by OH radicals in these rich flames with a rate constant at 1700 K of 9.2 (±1.5) × 10^{11} $cm^3/(mol \cdot s)$ as determined in the present experiments. As the acetylene decreases, methane rises with net yields which vary with the fuel used, reaching a maximum of 35% of the acetylene consumption for the ethylene flame. In the mechanism of Table I, CH_3 formation takes place through the reaction with H atoms of ketene, formed by the reaction of OH with C_2H_2, and CH_4 is in turn produced from the methyl radicals. As discussed in the text, alternative reaction mechanisms could also explain the data, and additional experiments are needed to clarify the reaction mechanism by which acetylene is consumed in rich flames.

Registry No. CH_4, 74-82-8; C_2H_2, 74-86-2; HO, 3352-57-6; C_2H_4, 74-85-1; C_3H_8, 74-98-6; CH_3, 2229-07-4; ketene, 463-51-4; allene, 463-49-0; propyne, 74-99-7; diacetylene, 460-12-8.

---

(16) Westbrook, C. K.; Pitz, W. J. *Combust. Sci. Technol.* **1984**, *37*, 117.

(17) Glarborg, P.; Miller, J. A.; Kee, R. J. *Combust. Flame* **1986**, *65*, 177.

(18) Spindler, K.; Wagner, H. Gg. *Ber. Bunsen-Ges. Phys. Chem.* **1982**, *86*, 2.

(19) Berman, M. R.; Fleming, J. W.; Harvey, A. B.; Lin, M. C. *Symp. (Int.) Combust.*, [*Proc.*], *19th* **1982**, 73.

(20) Husain, D.; Newton, D. P. *J. Chem. Soc., Faraday Trans. 2* **1982**, *78*, 51.

(21) Frank, P.; Bhaskaran, K. A.; Just, Th. *Symp. (Int.) Combust.*, [*Proc.*], *21st* **1986**, 885.

(22) Radhakrishnan, K.; Burcat, A. *Combust. Sci. Technol.* **1987**, *54*, 85.

(23) Tully, F. P. *Chem. Phys. Lett.* **1988**, *143*, 510.

(24) Tully, F. P.; Ravishankara, A. R.; Carr, K. *Int. J. Chem. Kinet.* **1983**, *15*, 1111.

(25) Stewart, P. H.; Larson, C. W.; Golden, D. M. *Combust. Flame* **1989**, *75*, 25.

(26) Atkinson, R. *Chem. Rev.* **1986**, *86*, 69.

(27) Kakumoto, T.; Ushirogouchi, T.; Saito, K.; Imamura, A. *J. Phys. Chem.* **1987**, *91*, 183.

(28) Perry, R. A. *Combust. Flame* **1984**, *58*, 221.

(29) Hatakeyama, S.; Honda, S.; Washida, N.; Akimoto, H. *Bull. Chem. Soc. Jpn.* **1985**, *58*, 2157.

(30) Vandooren, J.; Van Tiggelen, P. J. *Symp. (Int.) Combust.*, [*Proc.*], *16th* **1977**, 1133.

(31) Frank, P.; Bhaskaran, K. A.; Just, Th. *J. Phys. Chem.* **1986**, *90*, 2226.

(32) Warnatz, J. *Combust. Sci. Technol.* **1983**, *34*, 177.

(33) Stull, D. R.; Westrum, E. F.; Sinke, G. C. *The Chemical Thermodynamics of Organic Compounds*; Wiley: New York, 1969.

(34) Burcat, A. In *Combustion Chemistry*; Gardiner, W. C., Ed.; Springer-Verlag: New York, 1984; p 455.